BIOPHYSICS

Graphene biointerfaces for optical stimulation of cells

Alex Savchenko,[1]* Volodymyr Cherkas,[2,3] Chao Liu,[4†] Gary B. Braun,[5] Alexander Kleschevnikov,[6] Yury I. Miller,[4] Elena Molokanova[7]*

Copyright © 2018 The Authors, some rights reserved; exclusive licensee American Association for the Advancement of Science. No claim to original U.S. Government Works. Distributed under a Creative Commons Attribution NonCommercial License 4.0 (CC BY-NC).

Noninvasive stimulation of cells is crucial for the accurate examination and control of their function both at the cellular and the system levels. To address this need, we present a pioneering optical stimulation platform that does not require genetic modification of cells but instead capitalizes on unique optoelectronic properties of graphene, including its ability to efficiently convert light into electricity. We report the first studies of optical stimulation of cardiomyocytes via graphene-based biointerfaces (G-biointerfaces) in substrate-based and dispersible configurations. The efficiency of stimulation via G-biointerfaces is independent of light wavelength but can be tuned by changing the light intensity. We demonstrate that an all-optical evaluation of use-dependent drug effects in vitro can be enabled using substrate-based G-biointerfaces. Furthermore, using dispersible G-biointerfaces in vivo, we perform optical modulation of the heart activity in zebrafish embryos. Our discovery is expected to empower numerous fundamental and translational biomedical studies.

INTRODUCTION

Electrical signaling plays a central role in many aspects of cellular physiology, including excitability, ion homeostasis, regulation of protein expression, and cell proliferation. The ability to modulate electrical signaling by changing the cell membrane potential can provide the opportunity to control the functional state of a cell and, by extension, the activity of a whole organ. Technological tools enabling this control should not interfere with either the structural integrity of a cell or its genetic content. This key requirement presents a significant challenge. For example, selected electrical stimulation methods could have potential detrimental effects on cell health and integrity resulting from accompanying redox effects due to Faradaic processes (*1*) or disruption of the cell membrane by penetrating electrodes (*2*). Optical stimulation, including optogenetics, is considerably more cell friendly. Unfortunately, optogenetic stimulation requires high-level expression of exogenous transmembrane ion-conducting proteins (*3*–*5*) [that is, optogenetic actuators (*6*)], which means that the investigator has to change a cell to be able to control its behavior. These changes in the physiology and phenotypes of cells can be confounding in studies of cellular maturation, development, and disease progression, when the cell itself is undergoing drastic changes.

To address the challenge of developing a truly noninvasive stimulation method, we turned our attention to graphene and its unique combination of electronic, optical, and mechanical properties (*7*). Graphene can efficiently convert light into electricity via a hot-carrier multiplication process on a femtosecond time scale (*8*–*10*), which makes graphene very attractive for emerging applications in photonics and optoelectronics (*11*). Our pioneering solution to the "noninvasive cellular stimulation" challenge is a graphene-based light-controlled actuator positioned outside a genetically and structurally intact cell (Fig. 1A). This platform is fundamentally different from existing graphene applications aimed at sensing existing biological activity (*12*, *13*), because here, for the first time, graphene will play a proactive role in regulating the functional cellular activity.

[1]Department of Pediatrics, University of California, San Diego, La Jolla, CA 92093, USA. [2]Department of Molecular Biophysics, Bogomoletz Institute of Physiology, Kiev, Ukraine. [3]Department of Cellular Neurophysiology, Hannover Medical School, Hannover, Germany. [4]Department of Medicine, University of California, San Diego, La Jolla, CA 92093, USA. [5]STEMCELL Technologies, Vancouver, British Columbia, Canada. [6]Department of Neurosciences, University of California, San Diego, La Jolla, CA 92093, USA. [7]Nanotools Bioscience, San Diego, CA 92121, USA. *Corresponding author. Email: emolokanova@nanotoolsbio.com (E.M.); asavtchenko@ucsd.edu (A.S.)
†Present address: Synthesis and Editing Platform, China National Genebank, Shenzhen, China.

RESULTS

Substrate-based optoelectronic G-biointerfaces

We engineered substrate-based G-biointerfaces by depositing either pristine graphene or chemically converted graphene [reduced graphene oxide (rGO)] (*14*) on pretreated glass coverslips (see the Supplementary Materials for details). Cardiomyocytes (CMs) were cultured on G-coated substrates for several weeks, and their interfacing was evaluated using scanning electron microscopy (SEM) (Fig. 1B), light microscopy, and electrophysiology. We found that the cell density was significantly higher on G-coated substrates than on control substrates (Fig. 1C and fig. S1A), whereas the cell viability (fig. S1B) and contractile profiles were similar in both conditions. The excellent biocompatibility demonstrated by our G-biointerfaces is in agreement with previous studies (*13*) that used graphene as a support structure in cellular scaffolds. These studies suggested that the surface chemistry, mechanical properties, and microscale topographic features of graphene (*15*) are responsible for ensuring a favorable cell microenvironment.

To test the validity of our idea of a graphene-based optical actuator, we first examined the effects of light on the functional activity of CMs that had been cultured on control and G-coated substrates for 2 to 4 weeks (that is, long-term interfacing; Fig. 1, D and G). By performing electrophysiological experiments on individual CMs, we discovered that light illumination (green, 2.1 mW/mm^2) did not affect CMs (n = 5 cells) on control substrates but triggered membrane depolarization in CMs (n = 7 cells) on G-coated substrates, leading to action potential generation or the increase in action potential frequency (Fig. 1, E and H). These findings establish that graphene materials are capable of playing an active role in cell physiology by enabling light-controlled dynamic manipulation of cellular activity.

To visualize optical stimulation effects in multiple CMs, we evaluated their contractile kinetics using a label-free method by taking advantage of the high optical transparency of G-coated substrates [97.2 ± 0.5% for single-layer graphene (n = 8), 94.2 ± 1.8% for double-layer graphene (n = 8), and 86.2 ± 3.7% for rGO (n = 12)] and performing experiments using bright-field microscopy. We discovered that light (green, 4.6 mW/mm^2) produced fast and reversible changes in the contraction

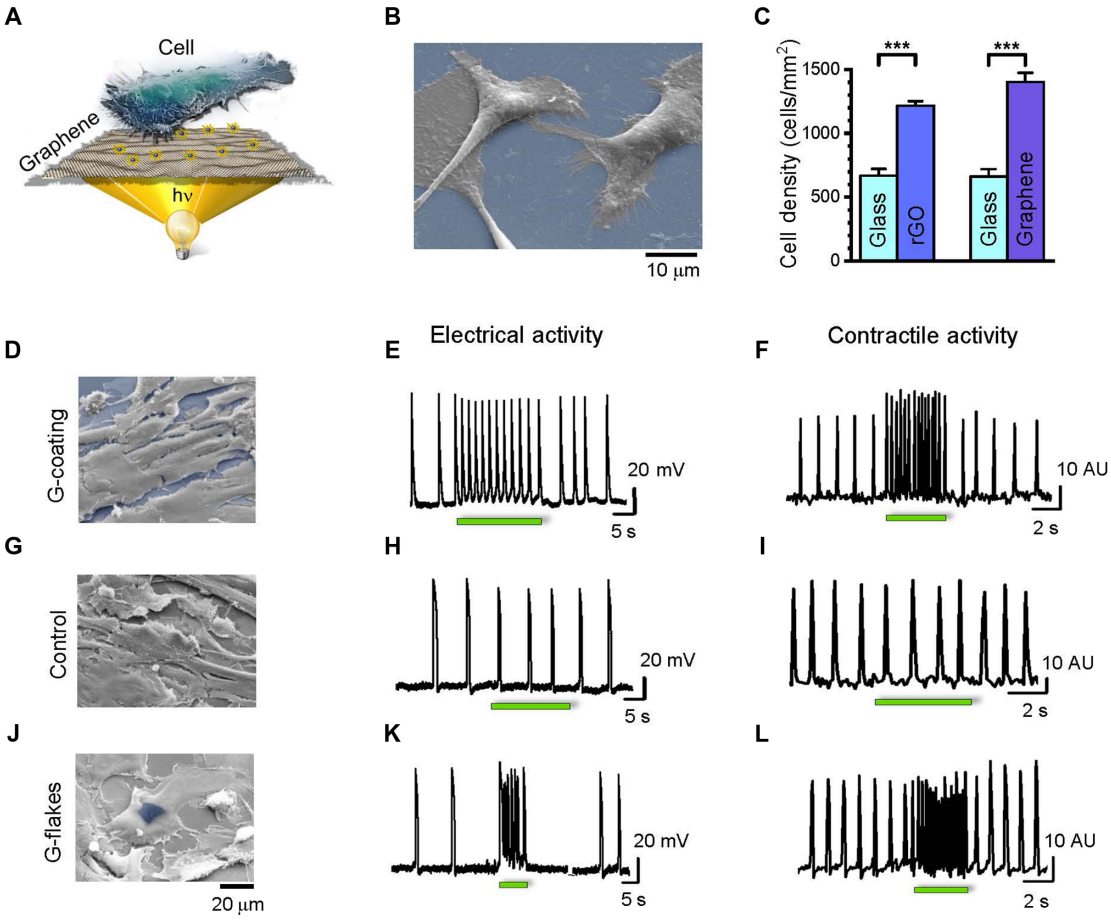

Fig. 1. Graphene-based optoelectronic interface for optical stimulation of cells. (**A**) Schematic representation of our hypothesis. (**B**) Representative scanning electron microscopy (SEM) image of iCell cardiomyocytes (CMs) on reduced graphene oxide (rGO)–coated coverslips. (**C**) Summary of the normalized cell density for neonatal rat ventricular CM cultures on control, rGO-coated, and graphene-coated coverslips. Data are means ± SEM ($n \geq 100$ cells per each condition). ***$P < 0.005$, unpaired t test. Representative SEM images of iCell CMs on rGO-coated (**D**) and control (**G**) coverslips, as well as CMs with an acutely deposited rGO flake (**J**). Representative traces demonstrating light-induced effects on action potentials in iCell CMs on rGO-coated (**E**) and control (**H**) coverslips and with deposited rGO flakes (**K**). Representative traces demonstrating light-induced effects on contractile activity of human-induced pluripotent stem cell (hiPSC)–derived CMs on rGO-coated (**F**) and control coverslips (**I**) and with deposited rGO-flakes (**L**). Graphene materials are highlighted blue. Light illumination events are indicated by bars. AU, arbitrary units.

frequency of spontaneously active CMs (movie S1) on rGO-coated substrates ($n = 282$ cells from 48 samples; Fig. 1F), whereas CMs on control substrates ($n = 46$ cells from 10 samples) were not affected (Fig. 1I). All active CMs were contracting synchronously and at the same rate, and light illumination affected their contraction frequency in the similar manner. Moreover, light illumination led to the initiation of contractions in several quiescent CMs on rGO-coated substrates.

Dispersible optoelectronic G-biointerfaces

In addition to the substrate-based configuration, G-biointerfaces can also be acutely applied to cells as dispersible structures. This approach would be particularly beneficial in intact tissues and cultures with nonuniform organization and when instant control over cellular activity is required. We explored a short-term cell-graphene interfacing paradigm by directly depositing multilayer rGO flakes on CMs that had been cultured on noncoated coverslips (Fig. 1J). We did not preselect rGO flakes based on their size/the number of layers, and therefore, the rGO-flake population exhibited broad size and thickness distributions (fig. S2). In our experimental conditions, the number of layers in rGO flakes was, on average, higher than 10, and these flakes usually have limited mechanical conformity (*16*). We expected cell-flake interfacing to be suboptimal because of the stochastic nature of flake deposition and the poor match between the curvature of a flake and the shape of a CM. Surprisingly, when we tested the electrical activity of individual CMs near flakes ($n = 4$ cells), we found that light illumination produced fast and reversible changes in action potential generation patterns (Fig. 1K). We performed label-free bright-field optical monitoring of contraction kinetics of multiple CMs and confirmed that, even under imperfect interfacing conditions, dispersible G-biointerfaces were able to efficiently increase the CM contraction frequency ($n = 56$ cells; Fig. 1L and movie S2). Efficient interfacing of dispersible G-biointerfaces with cells and their small size offers an exciting opportunity to use them in in vivo applications to mimic or augment endogenous activation triggers. In addition, dispersible G-biointerfaces can be beneficial when spatially constrained cellular stimulation is required.

Potential mechanisms underlying optical stimulation via G-biointerfaces

How does light illumination of G-biointerfaces lead to stimulation of cells? To answer this question, we started by probing for photogenerated

electrons in light-exposed G-biointerfaces using ultraviolet-visible (UV-Vis) spectroscopy and resazurin, an indicator of photocatalytic activity (*17*). In the presence of photogenerated electrons, resazurin (an absorption peak at 610 nm) irreversibly undergoes the reductive N-deoxygenation into resorufin (an absorption peak at 585 nm). Therefore, this photocatalytic reaction can be detected by monitoring the changes of absorbance at 610 nm. We found that, whereas light illumination (0.9 mW/mm^2) did not change absorption of resazurin deposited on noncoated glass coverslips, resazurin on G-biointerfaces was reduced in ~12 min (Fig. 2A), thus confirming the photogeneration of electrons and their efficient distribution from G-biointerfaces into aqueous solutions.

Next, we considered whether optical stimulation via G-biointerfaces is mediated by Faradaic (that is, charge transfer between photogenerated electrons and chemical species in the electrolyte solution) or capacitive (that is, charge redistribution) processes. When Faradaic charge transfer occurs, it is accompanied by redox reactions, resulting in changes in the solution pH value (*1*). Note that such Faradaic reaction as electrolysis of water has a standard potential of 1.23 V versus 70 mV for resazurin reduction (*18*). We found that the pH of electrolytic solution containing immersed G-coated coverslips did not change during continuous 30-min light illumination (Fig. 2C), strongly suggesting that the Faradaic mechanism (*1*, *19*) is not involved here. Furthermore, because we did not apply a voltage bias and the lifetime of photogenerated electrons in graphene is in the femtosecond range (*20*, *21*), photogenerated currents are expected to be negligible.

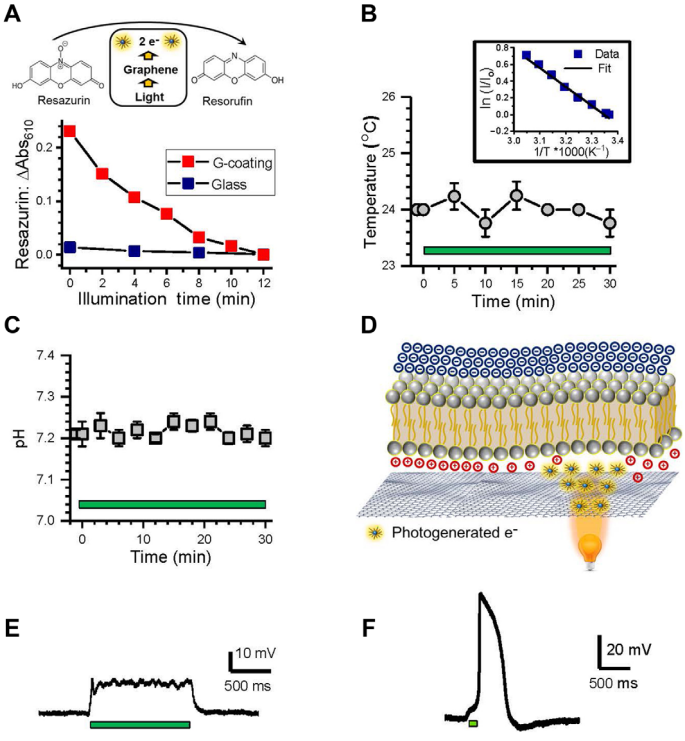

Fig. 2. Proposed mechanism of optical stimulation via G-biointerfaces. (**A**) Photogenerated electrons from G-biointerfaces are detected using UV-Vis spectroscopy that monitors changes in absorption spectra due to G-biointerface–mediated photocatalytic reduction of resazurin to resorufin (top). Graph shows changes in absorption of a 40 μM resazurin solution (at its absorption peak of 610 nM) on G-biointerfaces (red squares) or noncoated glass coverslips (blue circles) as a function of illumination time (465 nm, 1.8 mW/mm^2). (**B**) No changes in the surface temperature of rGO-coated coverslips during continuous 30-min light exposure (n = 3). Inset: Linear calibration curve was fitted to enable the subsequent extraction of the temperature values from the pipette resistance values. Light in (B) and (C): cyan, 4.3 mW/mm^2. Data are presented as mean ± SEM. (**C**) No changes in the pH values of an electrolytic solution covering rGO-coated coverslips during continuous 30-min light exposure (n = 5). (**D**) Cartoon illustrating the proposed mechanism of cellular optical stimulation using light-activated G-biointerfaces. (**E**) Representative trace of light-triggered membrane depolarization in a current-clamped CHO cell cultured on G-coated substrates. (**F**) Representative trace of light-triggered action potential in a current-clamped hiPSC-derived CM cultured on G-coated substrates. Light in (E) and (F): cyan, 4.5 mW/mm^2. Light illumination events are indicated by bars.

The capacitative mechanism of extracellular cellular stimulation is based on light-induced charge redistribution near the graphene/electrolyte and electrolyte/cell membrane interfaces (*1*, *19*). Negative charges positioned outside the cell membrane shift the extracellular area to relatively more negative potentials, which effectively translates into cell membrane depolarization and leads to the initiation of voltage-dependent processes in a cell. Note that the current profile during this stimulation is determined solely by the properties of a cell (for example, a constellation of endogenous voltage-gated ion channels and their voltage-dependent properties) because ion currents are derivatives of the depolarization event in this stimulation configuration.

One potential scenario of optical stimulation involves a charge redistribution due to temperature gradients induced by local heating (*22*, *23*). In our settings, direct light-induced, heat-mediated effects are unlikely because (i) a light intensity approximately 1000 times higher would be required for these effects (*6*, *22*, *23*) and (ii) light-induced heat usually produces a gradually changing cellular response during continuous light exposure (*22*), whereas we observed a rapidly achieved steady-state response. Furthermore, we found no changes in the surface temperature of G-coated coverslips during 30-min continuous light illumination (Fig. 2B). This finding was expected because graphene is a highly efficient light-to-electricity converter, and because of zero band gap and strong electron-electron interactions in graphene, photogenerated electrons are poorly coupled to the graphene surface and preferentially distribute their energy to multiple secondary electrons rather than produce lattice heating (*8*, *9*, *24*).

Optical stimulation via G-biointerfaces is more consistent with capacitive effects of "clouds" of photogenerated hot ballistic electrons from graphene (*24*), although this hypothesis requires further study. In the hypothesized scenario, ejected electrons (with a mean free path of up to 1 μm) displace cations near the graphene/cell membrane interface due to capacitive coupling between the cell membrane and the graphene surface (Fig. 2D), resulting in membrane depolarization. The kinetics of this process is controlled by light and determined by the femtosecond lifetime of photogenerated electrons (*20*, *21*). Because there is no accumulation of electrons, light illumination is expected to produce fast and reversible steady-state depolarization. This supposition was confirmed by whole-cell current-clamp experiments on nonexcitable Chinese hamster ovary (CHO) cells (Fig. 2E). In excitable cells, above-threshold depolarization results in action potential generation, as demonstrated by performing optical stimulation of current-clamped CMs on G-biointerfaces (Fig. 2F).

Optical properties of G-biointerfaces

To realize the full potential of G-biointerfaces, we proceeded with characterizing their properties and establishing the parameters of actuating light signals. The ability to use any light wavelength for optical stimulation

provides greater experimental flexibility, including using red light for deeper tissue penetration in vivo. We exposed CMs on rGO-coated substrates to cyan, green, and red light (1.2, 1.1, and 1 mW/mm^2, respectively) and determined that light signals of comparable intensities but different wavelengths produce similar effects on contractile activity (Fig. 3A). This finding is consistent with the fact that photon absorption in undoped graphene is nearly constant for wavelengths in the range from 300 to 2500 nm (Fig. 3B) (*25*). Thus, the efficiency of optical stimulation via G-biointerfaces is virtually independent of the light wavelength, and this property represents a significant advantage over optogenetics.

To investigate how varying the number of graphene layers affects the optical stimulation efficiency, we compared light-induced effects in CMs cultured on rGO-coated (five to six layers as estimated from optical transparency measurements) and graphene-coated substrates (one to two layers for single- or double-layer graphene). rGO-coated coverslips mediated more robust light-induced changes in contractile activity than graphene-coated coverslips (Fig. 3C). This finding is consistent with photon absorption being proportionate to the number of graphene layers (*26*) and provides an easily implemented method of tuning optical stimulation.

Both long ("step") and short ("pulsed") light illumination protocols can be useful for cell stimulation. With G-biointerfaces, the prolonged duration of illumination above the electron lifetime cannot produce an increase in depolarization amplitude (Fig. 2E) due to the femtosecond lifetime of photogenerated electrons in graphene. We demonstrated that, by selecting appropriate illumination parameters, it is possible to achieve similar stimulation of CMs on G-biointerfaces using a light signal of the same wavelength and intensity (Fig. 3D).

By varying the light intensity from 0.1 to 4.6 mW/mm^2, we determined that, at intensities above 1 mW/mm^2, rGO-coated substrates reliably stimulated CMs (Fig. 3E) and exhibited a linear dynamic range of operation (Fig. 3F). Intensities below a certain threshold (<0.4 mW/mm^2) were usually insufficient for CM stimulation. Therefore, by tuning the light intensity, it is possible to achieve a desired contraction frequency in any given population of CMs.

Biomedical applications for optical stimulation via G-biointerfaces

Numerous in vitro biomedical applications could benefit from graphene-based optical stimulation. For example, incorporating cell stimulation technologies during drug screening assays would allow for the development of more efficient drugs with complex mechanisms of action faster and reduce the costs associated with their development (*27*). Accurate pharmacological profiling needs the ability to dynamically modulate the frequency of the cellular activity, because at faster stimulation rates, use-dependent drugs exhibit greater effects and arrhythmic effects can be more pronounced (*27*). Optogenetic stimulation is not well suited for drug screening, because the overexpression of genetically encoded actuators in cells of interest can greatly affect ion homeostasis and distort drug effects (*28*–*30*). We explored the utility of G-biointerfaces for probing the effects of mexiletine, a sodium channel inhibitor with well-known use-dependent properties. By illuminating CMs on G-biointerfaces with light of different intensities, we were able to drive CM contraction frequency from spontaneous (<1.5 Hz) to various light-induced rates in the presence of 20 μM mexiletine (Fig. 4A). We determined that there was a strong, positive correlation between inhibitory effects of mexiletine

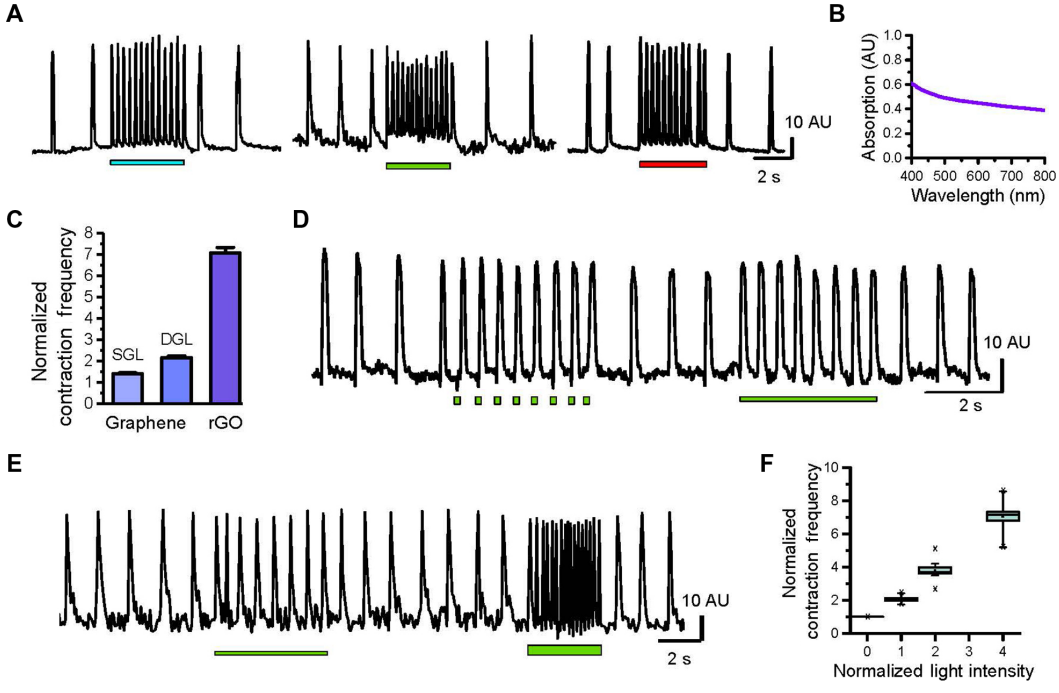

Fig. 3. Dynamic control of functional activity of CMs on G-biointerfaces. (**A**) Effects of cyan, green, and red light signals on contractile activity of iCell CMs on rGO-coated coverslips. (**B**) Absorption spectrum of rGO coating. (**C**) Light-induced effects in iCell CMs on coverslips (n = 14 per each condition) coated with single-layer graphene (SGL), double-layer graphene (DGL), and rGO. Data are means ± SEM. (**D**) Representative traces of light-induced changes in contractions of hiPSC-derived CMs on rGO-coated coverslips in response to 40-ms 2-Hz light pulses and a 3-s step of light (green, 1.1 mW/mm^2). (**E**) Representative traces demonstrating the effects of light signals of different intensities on iCell CMs on rGO-coated coverslips. (**F**) Box plots of light-induced changes in the contraction frequency (normalized to values at x = 0) as a function of light intensity. Light illumination events are indicated by bars. AU, arbitrary units.

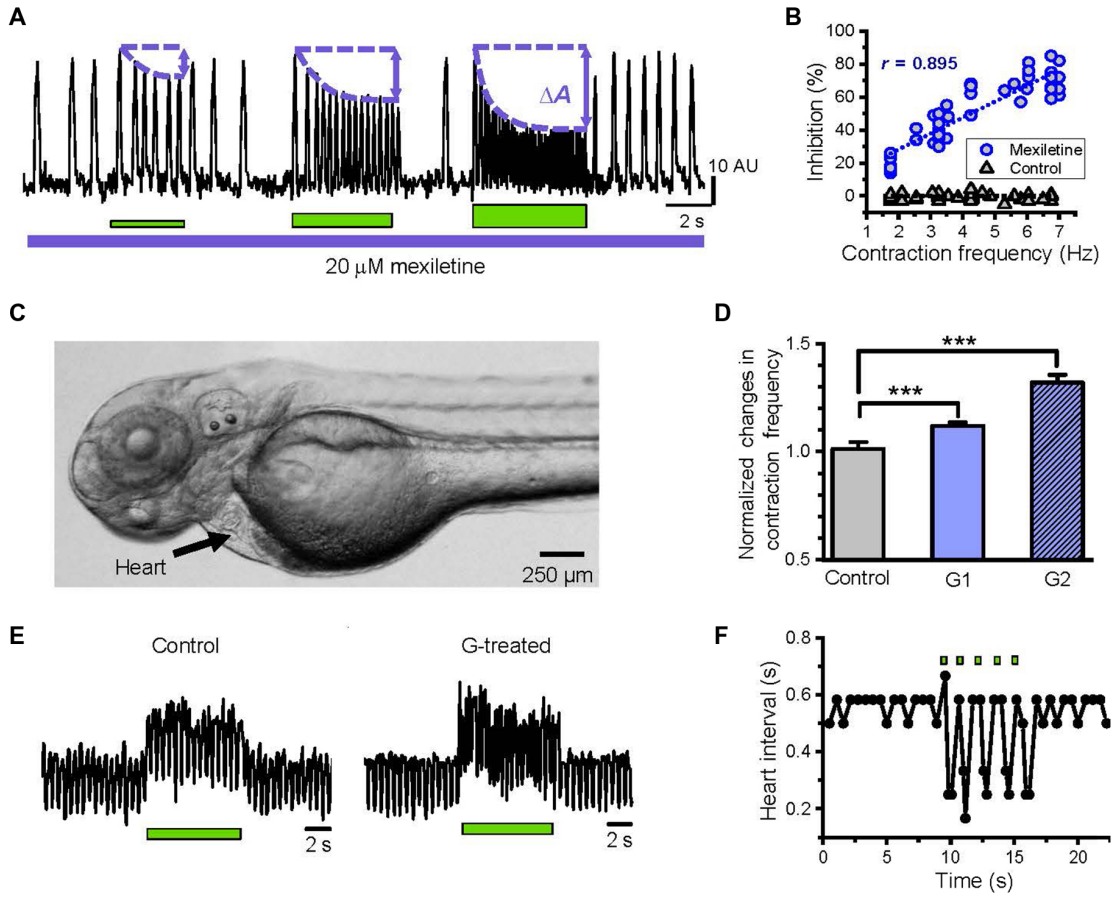

Fig. 4. Biological applications for G-biointerface–enabled optical stimulation. (**A**) Representative contraction traces in iCell CMs on light-illuminated G-coated coverslips in the presence of 20 μM mexiletine. Δ*A*, a mexiletine-induced decrease in the contraction amplitude at a given frequency; AU, arbitrary units. Dotted lines highlight the time course of use-dependent inhibition of CM contraction by mexiletine. (**B**) Summary of use-dependent effects of mexiletine in optically stimulated CMs: Inhibition in the absence (black triangles, $n = 36$) and the presence of mexiletine (blue circles, $n = 41$). *r*, Pearson's correlation coefficient (Pearson's correlation two-tailed *t* test). (**C**) Zebrafish embryo 3 dpf. (**D**) Summary of G-biointerface–enabled optical stimulation effects (green light, 0.8 mW/mm^2) on the heart rates of zebrafish embryos from three groups: Control ($n = 12$), injected with 0.1 mg/ml ($n = 6$, G1) and with 0.5 mg/ml ($n = 6$, G2). Data are presented as mean ± SEM. ***$P < 0.005$, paired *t* test. (**E**) Representative heart contraction traces demonstrating optical stimulation effects (green light, 0.8 mW/mm^2) in control (left) and G-treated (0.5 mg/ml; right) zebrafish embryos. (**F**) Heart periods from G-treated (right) zebrafish embryos stimulated by short 500-ms light pulses (2 mW/mm^2). Light illumination events are indicated by bars.

and the CM contraction frequency ($r = 0.895$, $n = 41$, $P < 0.001$; Fig. 4B), consistent with published data (*31*). By providing cellular stimulation during drug screening assays, G-biointerfaces could enable physiologically relevant assays and provide more predictive evaluation of drug-induced proarrhythmia risks in stem cell–derived CMs, as recommended by the emerging Comprehensive In Vitro Proarrhythmia Assay initiative (CiPA) (*27*, *32*).

To evaluate G-biointerfaces in in vivo settings, we used the zebrafish (*Danio rerio*), a well-established animal model for biomedicine and drug discovery (*33*, *34*). Critically, zebrafish embryos are optically transparent, which allows performing optical stimulation experiments on intact animals. In our experiments, zebrafish embryos at 3 days post-fertilization (dpf; Fig. 4C) were injected with phosphate-buffered saline (PBS; control) or rGO dispersion (0.1 or 0.5 mg/ml) in PBS (G-treated). We found that the basal heart rates were similar in control and G-treated groups (fig. S3), and all, but one, zebrafish retained full viability 3 days after injection, which confirms biocompatibility of G-biointerfaces. When we evaluated the effects of prolonged and pulsed light illumination steps on heart contractions using bright-field microscopy, we discovered that optical stimulation of G-treated zebrafish hearts resulted in a significant increase of the heart rate, whereas illumination of control zebrafish had no effect on their heart contractions (Fig. 4, D to F). Light-induced changes in heart contractions of G-treated zebrafish (movie S3) occurred fast and were dependent on rGO concentration (Fig. 4D).

DISCUSSION

Our results suggest that G-biointerfaces can offer an effective solution for a noninvasive cell stimulation challenge. G-biointerfaces have fundamental advantages over other optoelectronic stimulation platforms. These nanotechnology-based platforms (*27*) require a voltage bias and associated electrical equipment [silicon wafers (*35*)], layered architecture of electron- and hole-conducting materials to enable charge separation [conducting polymers (*19*)], or immediate proximity to the cell membrane to ensure sufficient "reach" of quantum-confined photogenerated electrons [semiconductor nanoparticles (*27*, *36*)]. Multiple shortcomings, ranging from (i) poor compatibility with optical detection

modalities due to low transparency, (ii) manufacture and miniaturization problems due to their mechanical properties and complex architecture, and (iii) inadequate biocompatibility, have precluded the widespread use of these platforms in biological and tissue engineering applications.

The physical properties of graphene are fundamentally different from the materials described above. Graphene is a zero–band gap semiconductor (that is, neither metal nor semiconductor), and its electrons behave as "massless" quasiparticles. In graphene, light produces hot ballistic charge carriers (*8*) that transfer their energy through a very efficient carrier-carrier scattering process, leading to multiple hot-carrier generation over a wide range of light frequencies. In addition, the mean free path of photogenerated hot ballistic electrons can be up to 1 μm (*37*), which provides enhanced flexibility in spatial positioning of G-biointerfaces near cells and explains the high efficiency of optical cell stimulation using dispersible G-biointerfaces with random geometry.

We anticipate that optical stimulation via G-biointerfaces could become a next-generation disruptive technology with a very wide range of innovative biomedical applications, including (i) empowering in vitro studies of activity- and voltage-dependent processes in the brain and heart and, eventually, aiding with the diagnosis and treatment of neurological and cardiovascular disorders; (ii) enabling activity-dependent production of more mature stem cell–derived cells; (iii) enhancing the predictiveness of engineered in vitro tissue models for drug discovery and cardiotoxicity; (iv) improving the outcome of functional integration of stem cell–derived cells into damaged tissues; (v) restoring vision; and (vi) fighting cardiac arrhythmias by acting as optical pacemakers.

MATERIALS AND METHODS

Materials

Graphene synthesis

Graphene was synthesized on 25-μm-thick copper foils (99.8%; Alfa Aesar, 13382) with the dimensions of 10 cm × 11 cm. Before the growth of graphene, the copper foils were cleaned by the following procedure: soaking in a shallow acetone bath, mechanical cleaning in acetone, transferring into a similar bath filled with isopropyl alcohol (IPA), mechanical cleaning in IPA, drying in a stream of compressed air, electropolishing, rinsing with deionized (DI) water and IPA, and blow-drying under a stream of compressed air. Atmospheric-pressure chemical vapor deposition (CVD) graphene synthesis was performed in a quartz tube furnace (MTI OTF-1200X-HVC-UL) with the following tube dimensions: diameter (d) = 7.6 cm and length (l) = 100 cm. The CVD chamber and the reactor gas-supply lines were purged of air for 5 min by flowing a mixture of all synthesis gases (hydrogen, methane, and argon) at their maximum flow rates while pulling vacuum on the chamber with a diaphragm vacuum pump. After 5 min, the gas flow was stopped, and the chamber was evacuated to about 10^{-4} torr with a turbomolecular vacuum pump to remove methane and hydrogen from the gas-mixing and the reactor chambers and to desorb the possible organic contaminants from the surface of the copper foil. The chamber was then repressurized to atmospheric pressure with ultrahigh purity argon [700 standard cm^3/min (SCCM)], which flowed constantly throughout the entire procedure of graphene synthesis. The copper foils were heated in argon flow to 1050°C (30 min). Upon reaching this temperature, additional hydrogen (60 SCCM) was flowed for 30 min to anneal and activate the copper substrate. After the 30 min of annealing, the flow rate of hydrogen was reduced to 5 SCCM, and 0.7 SCCM of methane was flowed for 20 min for the synthesis of graphene (total gas flow rate: 700 SCCM argon + 5 SCCM hydrogen + 0.7 SCCM methane = 705.7 SCCM). After 20 min of graphene growth, the furnace was turned off and cracked open at 5 cm (continuing the same gas flow). When the furnace cooled to 700°C (approximately 5 min) it was opened to 10 cm. At 350°C (approximately 30 min), the furnace was completely opened. At 200°C, the hydrogen and methane flows were cut off, and the reactor chamber was allowed to cool to room temperature in the argon flow (total cooling time was approximately 1 hour).

Reduction of graphene oxide

rGO was produced from graphene oxide (GO; Graphenea Inc.) by chemical reduction using L-ascorbic acid. First, 50 ml of aqueous GO dispersion (0.4 mg/ml) was sonicated for 1 hour at room temperature. To enable the colloidal stability of aqueous GO dispersions, the pH was adjusted to ~10 using 25% ammonia solution. GO dispersions were transferred into a glass beaker and agitated with a stir bar (225 rpm), and then, ascorbic acid (32 mg) was added. All chemicals are from Sigma-Aldrich. The GO-to-rGO reduction process was monitored by UV-Vis spectroscopy (NanoDrop 2000 UV-Vis spectrophotometer, Thermo Fisher Scientific) at regular time intervals. After 24 hours, the resultant rGO aqueous dispersion was aliquoted and washed four times with water through a process of centrifuging, decanting, and resuspending in water to the initial volume by sonication. Poly(vinylpyrrolidinone) (0.05% w/v) was added in the final rGO dispersion.

Fabrication of substrate-based G-biointerfaces

The initial substrate preparation included preparation of glass coverslips for G-coating. Specifically, glass coverslips (12 or 5 mm in diameter; VWR International) were cleaned using the Triton X-100 solution for 1 hour, thoroughly washed in DI water and ethanol, placed into KOH/hydrogen peroxide (1:1) for 1 hour, washed in DI water, and then dried in a 60°C oven for 10 min.

To prepare for transferring graphene onto glass coverslips, the copper foil bearing a film of CVD-grown graphene was first spin-coated with a 2.5% w/w solution of poly(methyl-methacrylate) (PMMA) in toluene at 4000 rpm for 60 s. After spin-coating, the exposed graphene on the side of the copper foil opposite the PMMA was etched using an oxygen plasma cleaner (30 s, 30 W, 200 mtorr oxygen pressure). Next, the PMMA/graphene-coated copper foil was floated in a bath of 1 M iron (III) chloride ($FeCl_3$) for 30 min to etch the copper. Then, the free-floating PMMA-supported graphene was transferred three times into DI water baths and then placed onto coverslips by "scooping" the free-standing film out of the DI water bath. After drying at room temperature for 2 hours, the coverslips were placed into an acetone bath overnight to remove the PMMA. Next, the coverslips were rinsed in IPA and dried in compressed air.

To produce rGO-based biointerfaces, glass coverslips were placed in Petri dishes filled with 2% (3-aminopropyl)triethoxysilane in ethanol for 15 min, thoroughly washed in ethanol, and cured at 110°C for 15 min. Subsequently, rGO was placed on glass coverslips by droplet deposition (for example, 10 μl per 12-mm coverslip). rGO-covered coverslips were air-dried and then placed in the cell culture hood for overnight sterilization with the UV light. Alternatively, we produced rGO-coated coverslips by (i) depositing GO droplets on glass coverslips as described above and then (ii) conducting the thermal reduction of GO directly on glass coverslips by placing them on a hot plate (T = 110° to 130°C) for 5 min. G-coated coverslips were stable when immersed into an extracellular physiological solution for up to 6 weeks.

rGO flakes on cells

The stock of rGO aqueous dispersion (2 mg/ml) was sonicated for 30 min, dispersed in extracellular solution, followed by 10-min sonication.

Subsequently, rGO dispersion was added to extracellular solution in wells with CMs, leading to final rGO concentrations of 0.02 to 0.1 mg/ml. rGO flakes were allowed approximately 30 min to fall to the bottom and settle on CMs before the start of optical stimulation experiments.

The structural parameters of rGO flakes were estimated using optical microscopy (Olympus IX71 fluorescent microscope) and subsequent image analysis (ImageJ software) by determining the dimensions of region of interests (ROIs) corresponding to single flakes and their optical transparency, as compared to ROIs located just outside flakes.

Temperature monitoring

Because of the temperature dependence of the electrolyte conductivity, local changes in temperature can be evaluated by monitoring the resistance of an open-patch pipette (*22*, *38*). A recoding chamber and patch pipettes were filled with a 200 mM NaCl aqueous solution, and G-coated coverslips were immersed into a recording chamber. To detect the local temperature, we positioned a patch pipette (~5 MΩ) as close as possible to a G-coated coverslip, applied current pulses (10 mV/MΩ) using an Axopatch 200B amplifier (Molecular Devices), and measured the pipette resistance while continuously illuminating G-coated coverslips with cyan light (4.3 mW/mm^2). To construct a calibration curve for the conversion from pipette resistance to temperature values, the solution in a chamber was preheated to 50°C, and then, the solution temperature and the pipette resistance were monitored simultaneously, while the solution was cooling down to the room temperature. The linear calibration curve was fitted to extract E_a, the electrolyte's activation energy, from the slope of the resulting Arrhenius plot. The conversion from pipette resistance to temperature values was performed using the equation $T_i = [1/T_0 - R/E_a \times \ln(R_0/R_i)]^{-1}$, where R is the gas constant, E_a is the electrolyte's activation energy, T_0 is the room temperature, T_i is the current temperature, R_0 is the resistance at T_0, and R_i is the resistance at T_i.

pH monitoring

G-coated coverslips were placed in MS-512 recording chambers (ALA Scientific Instruments) and covered by 100 μl of electrolytic solution composed of 124 mM NaCl, 3.0 mM KCl, 3.0 mM $CaCl_2$, 1.5 mM $MgCl_2$, 26 mM $NaHCO_3$, and 1.0 mM $NaH2PO_4$ (pH 7.2). This low-capacity electrolytic buffer was previously used to monitor small pH changes in neuronal slices (*39*). During continuous 30-min light illumination (cyan, 4.3 mW/mm^2) of G-coated coverslips immersed into electrolytic solution, we conducted pH measurements every 3 min using Orion Micro Automatic Temperature Compensation Probe (928007MD, Thermo Fisher Scientific), which has a minimum sample size of 10 μl and a precision of pH 0.02.

Cell culture

Neonatal rat ventricular CMs

Neonatal rat ventricular CMs were isolated using the neonatal rat CM isolation kit (Worthington) and cultured at 37°C with 5% CO_2. Briefly, ventricles were dissected from 1-day-old Hsd:SD rats (Sprague-Dawley) and then digested overnight at 4°C with trypsin. Digestion continued the following morning with collagenase for approximately 60 min at 37°C. Cells were preplated for 90 min to remove fibroblasts and plated on matrigel-coated cell culture dishes in high-serum media [Dulbecco's modified Eagle's medium/F12 (1:1), 0.2% bovine serum albumin, 3 mM sodium pyruvate, 0.1 mM ascorbic acid, transferrin (4 mg/liter), 2 mM L-glutamine, 100 nM thyroid hormone (T3) supplemented with 10% horse serum, and 5% fetal bovine serum (FBS)] at 2 × 10^5 cells/cm^2. After 24 hours, media was changed to low-serum medium (same as above but only with 0.25% FBS).

Mouse embryonic stem cell–derived CMs (mCMs^{ESC})

A stable mouse embryonic stem cell (mESC) line for drug resistance selection of CMs (*Myh6-Puro^r;Rex-Blast^r*) was generated by lentiviral transduction and blasticidin selection, similar to our previously reported human line (*40*). These cells were engineered with *αMHC-mCherry-Rex-Bla^r* construct, which expresses mCherry under αMHC promoter in CMs. mCMs^{ESC} were obtained by differentiation of *Myh6-Puro^r;Rex-Blast^r* mESCs in a differentiation media containing Iscove's modified Dulbecco media supplemented with 10% FBS, 2 mM glutamine, 4.5 × 10^{-4} M monothioglycerol, 0.5 mM ascorbic acid, transferrin (200 μg/ml; Roche), 5% protein-free hybridoma media (PFHM-II, Invitrogen), and antibiotics/antimycotic as embryoid bodies until day 4 and plated onto adherent cell culture plate until day 9, 1 day after the onset of spontaneous beating. To purify *Myh6$^+$* CMs, we added puromycin at differentiation day 9 for 24 hours. Subsequently, cells were trypsinized and plated as monolayer CMs.

iCell CMs (Cellular Dynamics International) are hiPSC-derived CMs. iCell CMs were thawed per the manufacturer's instructions. Twenty-five microliters of the cell suspension (160,000 cells/ml) was added to a gelatin-coated 384-well plate. The cells were then left undisturbed for 48 hours at 37°C with 5% CO_2. After 48 hours, 75 μl of chemically defined m was added to each well for a total of 100 μl, and then, the half of the volume was changed every other day. When CMs began their spontaneous contractions after 10 to 14 days in culture, they were lifted with trypsin and replated at a density of 500,000 cells per a 12-mm coverslip. CMs were cultured on coverslips for 2 to 3 weeks before experiments.

hiPSC-derived CMs

H9 line (WA09), a human embryonic stem cell (hESC) line, was supplied by WiCell Research Institute. hESCs were dissociated using a 0.5 mM EDTA in PBS without $CaCl_2$ or $MgCl_2$ for 7 min at room temperature. Cells were plated at 3.0 × 10^5 cells per well of a 12-well plate in mTeSR1 media (STEMCELL Technologies) supplemented with 2 μM thiazovivin (STEMCELL Technologies) for the first 24 hours after passage. Cells were fed for 3 to 5 days until they reached ≥90% confluence. Subsequently, cells were washed with PBS, and the medium was changed to the CDM media (*41*). For the first 48 hours of differentiation, the CDM media was supplemented with 6 μM of the glycogen synthase kinase–3 inhibitor CHIR99021 (Selleck). After 48 hours, the CDM3 media was supplemented with 2 μM Wnt-C59 (Selleck). Each subsequent 48 hours, this medium was replaced with basic CDM3 media. Plates were monitored daily and assessed for beating. Beating CMs can be seen as early as the sixth day of differentiation. On day 14, all wells containing pure cultures (<85%) were gently washed once with PBS. Five hundred microliters of TrypLE select enzyme (Gibco) was added to induce dissociation of cultures into single cells. After 5 min, dissociating cultures were dispersed by tapping on the plate with an open palm to facilitate dislodging. Dissociating cultures were gently collected to a 15-ml tube and then filtered through a 100 μM cell strainer (Fisher). An equal volume of RPMI media containing 10% FBS was added to inhibit enzyme activity. After that, cells were centrifuged at 0.1 relative centrifugal force for 4 min. Once pellets were obtained, the remaining solution was aspirated, and pellets were dispersed by gentle flicking. Cells were then gently resuspended in CDM3 media containing 10% knockout serum replacement (KOSR; Gibco) and 1 μM thiazovivin (STEMCELL Technologies). After the cell density was obtained by counting using a Bio-Rad TC20 cell counter, the desired dilutions were prepared. Cells

were replated at the desired density onto matrigel-coated plates in CDM3 supplemented with 10% KOSR and 1 μM Thiazovivin. After 48 hours, this media was replaced with normal CDM3 media. All cultures (primary, pluripotent, and differentiation) were maintained with 2 ml of medium per 9.6 cm^2 of surface area or equivalent. All cell cultures were routinely tested for mycoplasma contamination using the MycoAlert Kit (Lonza).

Scanning electron microscopy

To prepare samples for SEM, CMs were first washed with 0.1 M phosphate buffer (pH 7.4), fixed with 4% formaldehyde solution for 2 hours at room temperature, and then washed with the same buffer three times for 5 min each. Following dehydration with graded series of alcohol [35% ethanol (10 min), 50% ethanol (10 min), 75% ethanol (10 min), 95% ethanol (two changes in 10 min), 100% ethanol (three changes in 15 min)], all samples were freeze-dried in a vacuum chamber and coated with sputtered iridium. We acquired SEM images on the XL30 ESEM-FEG (FEI) at the working distance of 10 mm while using the 10-kV energy beam.

Cell viability assay

Cell viability was assessed using the LIVE/DEAD Viability/Cytotoxicity Kit (Life Technologies). This kit contains membrane-permeable calcein-AM (for detection of enzymatically active live cells, green fluorescence) and membrane-impermeable ethidium homodimer-1 (EthD-1; for detection of dead cells with compromised membrane, red fluorescence). G-coated and noncoated (for example, control) glass coverslips with CMs (n = 3 per experimental condition) were randomly placed into multiwell plates and then were incubated with 2 μM calcein-AM and 4 μM EthD-1 for 30 min per the manufacturer's protocol. Subsequently, images (n = 3 per coverslip) were randomly taken using the Olympus IX71 fluorescent microscope equipped with a QIClick charge-coupled device (CCD) camera (QImaging) and standard filters [fluorescein, rhodamine, and 4′,6-diamidino-2-phenylindole (DAPI) filters for calcein, EthD-1, and Hoechst signal detection, respectively]. The data were analyzed using ImageJ image analysis software by a person without the knowledge of the placement order of coverslips. The cell death was calculated as the percentage ratio of the number of EthD-1–positive cells divided by the sum of the numbers of EthD-1–positive and calcein-positive cells.

Electrophysiology

Whole-cell current-clamp recordings were performed at room temperature using the validated experimental protocol. Briefly, coverslips with cells were placed in an experimental chamber (RC-25-F, Warner Instruments) filled with an extracellular solution consisting of 150 mM NaCl, 5.4 mM KCl, 1.8 mM $CaCl_2$, 1 mM $MgCl_2$, 1 mM Na-pyruvate, 15 mM glucose, and 10 mM Hepes (pH 7.4). Patch pipettes with a final tip resistance of 3 to 6 MΩ were filled with a solution consisting of 150 mM KCl, 5 mM NaCl, 5 mM MgATP, 10 mM Hepes, 5 mM EGTA (pH 7.2). All recordings were acquired using a Digidata 1322 interface, an Axopatch 200B amplifier, and pClamp software (Molecular Devices). The data were digitally sampled at 10 kHz and filtered using an eight-pole Bessel analog low-pass filter at 2-kHz cutoff frequency.

Detection of photogenerated electrons

The redox dye resazurin has been routinely used for many years for detecting photocatalytic activity on different surfaces. Upon encountering photogenerated electrons, resazurin was reduced and irreversibly changed into resorufin. This process was accompanied by changes in absorption spectra, and therefore, it can be easily detected using digital photography or a plate reader: The maximum absorbance wavelengths were 610 nm for resazurin and 580 and 454 nm for resorufin. The stock solution of 4 mM resazurin was prepared by dissolving 1 g of resazurin sodium salt (Sigma-Aldrich) in 100 ml of sterile PBS, filtered it through a 0.22-μm sterile filter, and stored at +4°C until needed. After 1% resazurin solution was spin-coated or drop-casted on glass coverslips, all samples were subjected to repeated cycles of 2-min white light illumination (0.9 mW/mm^2). After each illumination event, absorption spectra of overcoated solution was acquired using Infinite 200 Pro plate reader (Tecan) or NanoDrop 2000 UV-Vis spectrophotometer (Thermo Fisher Scientific). The resazurin-to-resorufin conversion by photogenerated electrons from graphene was quantified by the change in absorbance at 610 nm as function of illumination time: $\Delta Abs_{610}(t)$ was calculated as the difference between the absorbance of the ink film at certain time points and after all resazurin had been converted into resorufin but before resorufin is further converted in the photocatalytic reaction to dihydroresorufin and other colorless products.

Imaging experiments

Imaging experiments were performed on an inverted Olympus IX71 microscope equipped with a QImaging QIClick CCD camera, an excitation light source X-Cite 120Q (Excelitas), and the set of excitation filters [485 ± 20 nm ("cyan"), 560 ± 20 nm ("green"), and 630 ± 40 nm ("red") (Chroma Technology Corp.)]. Raw movies were acquired at 30 frames per second (fps). Olympus cellSens Microscope Imaging Software was used for camera control and data acquisition.

In addition, to perform optical stimulation of CMs with pulsed and step-like light signals, we used ImageXpress Micro XLS System (Molecular Devices) equipped with a SPECTRA X light engine (Lumencor) and standard filter sets. Raw movies were acquired at 50 fps and analyzed using MetaXpress Imaging software (Molecular Devices). The light intensity measurements were performed using LumaSpec800 optical power meter (Prior Scientific).

Detection of CM contractions

We monitored spontaneous contractions of CMs using either Olympus IX71 or ImageXpress Micro XLS in bright-field mode. The "label-free" nature of this approach is highly advantageous because it allows to monitor cells noninvasively, repeatedly, and over long periods of time without any signal deterioration. To extract the data from raw movies, a user manually determined regions of interest (ROIs) that exhibited considerable contraction-driven intensity changes and plotted changes in intensity versus time (ImageJ software). The frequency was quantified by calculating the number of contractions per 1 s. Alternatively, raw movies with contracting CMs were processed by a custom-written automatic image analysis software (in MATLAB). Specifically, after video recordings were exported as a stack of TIFF files, the intensity of all pixels across a temporal domain was analyzed to select the areas with the maximum intensity variance (MIV) change over time. A subset of pixels that falls into top the 10% in terms of MIV was selected for subsequent tracking of CM movements. Pixel displacement was calculated as the square root of a sum of squares of x and y displacements multiplied by a pixel size, followed by subtraction of the weighted mean of the resting point coordinates at each time point. The contraction tracking was processed by the algorithm of maximum correlation search between the coordinates of an ROI around the active pixel subset and the same ROI of the weighted resting state. Cross correlation of displacement over time for each ROI was used to detect population(s)

of synchronously active cells. Synchronous active regions were averaged if threshold conditions are met (movie S4). Manual and automated analyses of the same contraction movies produced identical data sets for absolute values of contraction frequencies and relative changes in contraction amplitudes. The dependence of changes in CM contraction frequencies from the light intensity was presented in the box graph (Fig. 3F), where each box represents 50% of the data, the horizontal bar is the median, the closed symbol is the mean, and the error bars indicate the full range.

Mexiletine experiments

The contraction kinetics of iCell CMs (Cellular Dynamics International) treated with 20 μM mexiletine (Sigma) was monitored using a label-free bright-field imaging approach and analyzed using a custom-made imaging software described above. Mexiletine is an inhibitor of voltage-gated sodium ion channels. Because of the specifics of its binding kinetics, mexiletine can accumulate inside a channel pore if a channel closes faster than mexiletine can dissociate from a channel. This kinetics results in more pronounced inhibition at higher channel-opening frequencies or, in other words, use-dependent inhibition. Because drug accumulation is a gradual process, mexiletine-induced effects should be evaluated when inhibition reaches the steady state. Therefore, in our study, mexiletine-induced inhibition at any given frequency (Fig. 4B) was quantified by calculating a ratio between ΔA (arrows in Fig. 4A) and A_0, where $\Delta A = A_0 - A_{ss}$, A_0 is the amplitude of the first contraction, and A_{ss} is the contraction amplitude at the steady-state level.

Optical stimulation of zebrafish hearts

All animal studies were approved by the University of California, San Diego Institutional Animal Care and Use Committee. Adult wild-type (AB strain) zebrafish were maintained at 28°C (14-hour light/10-hour dark cycle) and fed with brine shrimp twice a day. Zebrafish embryos at 3 dpf were anesthetized in tricaine (168 μg/ml; Sigma, catalog no. A5050) and immobilized in a 0.5% low–melting point agarose gel (Sigma, catalog no. A9414). The stock of an aqueous rGO dispersion (2 mg/ml) was used in our experiments. After 20 min of sonication, 15 min of centrifugation, and subsequent dispersion in PBS, rGO was used at final concentrations of 0.1 to 0.5 mg/ml. Six nanoliters of PBS or rGO dispersion in PBS were injected through the cardinal vein above the heart chamber using a FemtoJet microinjector (Eppendorf). Before optical stimulation experiments, zebrafish embryos were allowed to equilibrate for at least 45 min.

To study optical stimulation effects, heart rate changes were induced by illumination with a 532-nm 5-mW laser (Pinty). Images and videos were captured using a Leica CTR5000 microscope equipped with a DFC310FX camera. The video capture mode was continuous at 12.4 fps. All videos were analyzed using Fiji image analysis software by selecting ROIs with contraction-driven changes in luminosity and subtracting background illumination.

To evaluate biocompatibility of G-biointerfaces, 3-dpf embryos were released from low–melting point agarose and kept in E3 medium until 6 dpf, without feeding. rGO-injected embryos developed normally, and no obvious detrimental effects were detected in the rGO-injected group, when compared with the PBS-injected control group.

Statistical analysis

Data are means ± SEM. Comparison of the data sets was performed using a two-tailed Student's *t* test or one-way analysis of variance (ANOVA) with a Bonferroni post hoc test, when appropriate. The results were considered statistically significant at probabilities $P < 0.05$. We determined the sample sizes in our experiments for the statistical power of 0.8, the statistical significance criteria of 0.05, and the prespecified effect size of 0.2 by performing "Power and sample size analysis" calculations using OriginPro 2015 software. Statistical analysis was performed using Prism 6 statistical software (Graph Pad Software Inc.) and OriginPro 2015 software (OriginLab).

SUPPLEMENTARY MATERIALS

Supplementary material for this article is available at http://advances.sciencemag.org/cgi/content/full/4/5/eaat0351/DC1

fig. S1. Biocompatibility of G-biointerfaces.
fig. S2. Geometrical characteristics of G-flakes.
fig. S3. Basal heart rates in control and G-treated zebrafish ($n = 7$ for each group) 2 hours after injection.
movie S1. Optical stimulation of contractile activity in mouse embryonic stem cell–derived CMs cultured on rGO-coated coverslips (green light, 4.6 mW/mm^2).
movie S2. Optical stimulation of contractile activity in mouse embryonic stem cell–derived CMs via rGO flakes using the same conditions as in movie S1.
movie S3. Effects of light illumination on the heart contractions in a 3-dpf zebrafish embryo injected with G-biointerfaces (0.5 mg/ml) dispersed in PBS.
movie S4. Automated image analysis of CM contractions.

REFERENCES AND NOTES

1. D. R. Merrill, M. Bikson, J. G. R. Jefferys, Electrical stimulation of excitable tissue: Design of efficacious and safe protocols. *J. Neurosci. Methods* **141**, 171–198 (2005).
2. E. Molokanova, A. Savchenko, Bright future of optical assays for ion channel drug discovery. *Drug Discov. Today* **13**, 14–22 (2008).
3. K. Deisseroth, Optogenetics: 10 years of microbial opsins in neuroscience. *Nat. Neurosci.* **18**, 1213–1225 (2015).
4. A. B. Arrenberg, D. Y. R. Stainier, H. Baier, J. Huisken, Optogenetic control of cardiac function. *Science* **330**, 971–974 (2010).
5. U. Nussinovitch, L. Gepstein, Optogenetics for in vivo cardiac pacing and resynchronization therapies. *Nat. Biotechnol.* **33**, 750–754 (2015).
6. A. C. Thompson, P. R. Stoddart, E. D. Jansen, Optical stimulation of neurons. *Curr. Mol. Imaging* **3**, 162–177 (2014).
7. A. K. Geim, K. S. Novoselov, The rise of graphene. *Nat. Mater.* **6**, 183–191 (2007).
8. N. M. Gabor, J. C. W. Song, Q. Ma, N. L. Nair, T. Taychatanapat, K. Watanabe, T. Taniguchi, L. S. Levitov, P. Jarillo-Herrero, Hot carrier–assisted intrinsic photoresponse in graphene. *Science* **334**, 648–652 (2011).
9. K. Tielrooij, J. C. W. Song, S. A. Jensen, A. Centeno, A. Pesquera, A. Zurutuza Elorza, M. Bonn, L. S. Levitov, F. H. L. Koppens, Photoexcitation cascade and multiple hot-carrier generation in graphene. *Nat. Phys.* **9**, 248–252 (2013).
10. J. C. Johannsen, S. Ulstrup, A. Crepaldi, F. Cilento, M. Zacchigna, J. A. Miwa, C. Cacho, R. T. Chapman, E. Springate, F. Fromm, C. Raidel, T. Seyller, P. D. C. King, F. Parmigiani, M. Grioni, P. Hofmann, Tunable carrier multiplication and cooling in graphene. *Nano Lett.* **15**, 326–331 (2015).
11. F. Bonaccorso, Z. Sun, T. Hasan, A. C. Ferrari, Graphene photonics and optoelectronics. *Nat. Photonics* **4**, 611–622 (2010).
12. D. Kuzum, H. Takano, E. Shim, J. C. Reed, H. Juul, A. G. Richardson, J. de Vries, H. Bink, M. A. Dichter, T. H. Lucas, D. A. Coulter, E. Cubukcu, B. Litt, Transparent and flexible low noise graphene electrodes for simultaneous electrophysiology and neuroimaging. *Nat. Commun.* **5**, 5259 (2014).
13. A. V. Zaretski, S. E. Root, A. Savchenko, E. Molokanova, A. D. Printz, L. Jibril, G. Arya, M. Mercola, D. J. Lipomi, Metallic nanoislands on graphene as highly sensitive transducers of mechanical, biological, and optical signals. *Nano Lett.* **16**, 1375–1380 (2016).
14. G. Eda, M. Chhowalla, Chemically derived graphene oxide: Towards large-area thin-film electronics and optoelectronics. *Adv. Mater.* **22**, 2392–2415 (2010).
15. T. Kim, Y. H. Kahng, T. Lee, K. Lee, D. H. Kim, Graphene films show stable cell attachment and biocompatibility with electrogenic primary cardiac cells. *Mol. Cells* **36**, 577–582 (2013).
16. S. Scharfenberg, D. Z. Rocklin, C. Chialvo, R. L. Weaver, P. M. Goldbart, N. Mason, Probing the mechanical properties of graphene using a corrugated elastic substrate. *Appl. Phys. Lett.* **98**, 091908 (2011).
17. A. Mills, J. Wang, M. McGrady, Method of rapid assessment of photocatalytic activities of self-cleaning films. *J. Phys. Chem. B* **110**, 18324–18331 (2006).
18. T. F. Guerin, M. Mondido, B. McClenn, B. Peasley, Application of resazurin for estimating abundance of contaminant-degrading micro-organisms. *Lett. Appl. Microbiol.* **32**, 340–345 (2001).

19. D. Ghezzi, M. R. Antognazza, M. D. Maschio, E. Lanzarini, F. Benfenati, G. Lanzani, A hybrid bioorganic interface for neuronal photoactivation. *Nat. Commun.* **2**, 166 (2011).
20. P. A. George, J. Strait, J. Dawlaty, S. Shivaraman, M. Chandrashekhar, F. Rana, M. G. Spencer, Ultrafast optical-pump terahertz-probe spectroscopy of the carrier relaxation and recombination dynamics in epitaxial graphene. *Nano Lett.* **8**, 4248–4251 (2008).
21. J. M. Dawlaty, S. Shivaraman, M. Chandrashekhar, F. Rana, M. G. Spencer, Measurement of ultrafast carrier dynamics in epitaxial graphene. *Appl. Phys. Lett.* **92**, 042116 (2008).
22. M. G. Shapiro, K. Homma, S. Villarreal, C.-P. Richter, F. Bezanilla, Infrared light excites cells by changing their electrical capacitance. *Nat. Commun.* **3**, 736 (2012).
23. M. W. Jenkins, A. R. Duke, S. Gu, Y. Doughman, H. J. Chiel, H. Fujioka, M. Watanabe, E. D. Jansen, A. M. Rollins, Optical pacing of the embryonic heart. *Nat. Photonics* **4**, 623–626 (2010).
24. M. Freitag, T. Low, F. Xia, P. Avouris, Photoconductivity of biased graphene. *Nat. Photonics* **7**, 53–59 (2013).
25. K. F. Mak, M. Y. Sfeir, Y. Wu, C. H. Lui, J. A. Misewich, T. F. Heinz, Measurement of the optical conductivity of graphene. *Phys. Rev. Lett.* **101**, 196405 (2008).
26. R. R. Nair, P. Blake, A. N. Grigorenko, K. S. Novoselov, T. J. Booth, T. Stauber, N. M. R. Peres, A. K. Geim, Fine structure constant defines visual transparency of graphene. *Science* **320**, 1308 (2008).
27. E. Molokanova, M. Mercola, A. Savchenko, Bringing new dimensions to drug discovery screening: Impact of cellular stimulation technologies. *Drug Discov. Today* **22**, 1045–1055 (2017).
28. G. T. Dempsey, K. W. Chaudhary, N. Atwater, C. Nguyen, B. S. Brown, J. D. McNeish, A. E. Cohen, J. M. Kralj, Cardiotoxicity screening with simultaneous optogenetic pacing, voltage imaging and calcium imaging. *J. Pharmacol. Toxicol. Methods* **81**, 240–250 (2016).
29. A. Klimas, C. M. Ambrosi, J. Yu, J. C. Williams, H. Bien, E. Entcheva, OptoDyCE as an automated system for high-throughput all-optical dynamic cardiac electrophysiology. *Nat. Commun.* **7**, 11542 (2016).
30. B. D. Allen, A. C. Singer, E. S. Boyden, Principles of designing interpretable optogenetic behavior experiments. *Learn. Mem.* **22**, 232–238 (2015).
31. J.-F. Desaphy, A. Dipalma, T. Costanza, R. Carbonara, M. M. Dinardo, A. Catalano, A. Carocci, G. Lentini, C. Franchini, D. C. Camerino, Molecular insights into the local anesthetic receptor within voltage-gated sodium channels using hydroxylated analogs of mexiletine. *Front. Pharmacol.* **3**, 17 (2012).
32. P. T. Sager, G. Gintant, J. R. Turner, S. Pettit, N. Stockbridge, Rechanneling the cardiac proarrhythmia safety paradigm: A meeting report from the Cardiac Safety Research Consortium. *Am. Heart J.* **167**, 292–300 (2014).
33. J. Bakkers, Zebrafish as a model to study cardiac development and human cardiac disease. *Cardiovasc. Res.* **91**, 279–288 (2011).
34. C. A. MacRae, R. T. Peterson, Zebrafish as tools for drug discovery. *Nat. Rev. Drug Discov.* **14**, 721–731 (2015).
35. Y. Goda, M. A. Colicos, Photoconductive stimulation of neurons cultured on silicon wafers. *Nat. Protoc.* **1**, 461–467 (2006).
36. T. C. Pappas, W. M. S. Wickramanyake, E. Jan, M. Motamedi, M. Brodwick, N. A. Kotov, Nanoscale engineering of a cellular interface with semiconductor nanoparticle films for photoelectric stimulation of neurons. *Nano Lett.* **7**, 513–519 (2007).
37. K. S. Novoselov, A. K. Geim, S. V. Morozov, D. Jiang, Y. Zhang, S. V. Dubonos, I. V. Grigorieva, A. A. Firsov, Electric field effect in atomically thin carbon films. *Science* **306**, 666–669 (2004).
38. J. Yao, B. Liu, F. Qin, Rapid temperature jump by infrared diode laser irradiation for patch-clamp studies. *Biophys. J.* **96**, 3611–3619 (2009).
39. N. Fedirko, N. Svichar, M. Chesler, Fabrication and use of high-speed, concentric H^+- and Ca^{2+}-selective microelectrodes suitable for in vitro extracellular recording. *J. Neurophysiol.* **96**, 919–924 (2006).
40. H. Kita-Matsuo, M. Barcova, N. Prigozhina, N. Salomonis, K. Wei, J. G. Jacot, B. Nelson, S. Spiering, R. Haverslag, C. Kim, M. Talantova, R. Bajpai, D. Calzolari, A. Terskikh, A. D. McCulloch, J. H. Price, B. R. Conklin, H. S. Vincent Chen, M. Mercola, Lentiviral vectors and protocols for creation of stable hESC lines for fluorescent tracking and drug resistance selection of cardiomyocytes. *PLOS ONE* **4**, e5046 (2009).
41. P. W. Burridge, E. Matsa, P. Shukla, Z. C. Lin, J. M. Churko, A. D. Ebert, F. Lan, S. Diecke, B. Huber, N. M. Mordwinkin, J. R. Plews, O. J. Abilez, B. Cui, J. D. Gold, J. C. Wu, Chemically defined generation of human cardiomyocytes. *Nat. Methods* **11**, 855–860 (2014).

Acknowledgments: We thank W. L. McKeithan, S. Spiering, C. Walquist, C. Hurtado, and K. Wei for help with CM cell culture; C. Bardy for help with preliminary electrophysiological experiments; A. Zaretski for help with graphene-related experiments; and M. Mercola for reading and making comments on the manuscript. **Funding:** This study was supported by American Heart Association grant 16POST2720126 (to C.L.), NSF grant 1746607 (to E.M.), and NIH grants HL135737 (to Y.I.M.) and R43TR001911 (to E.M.). **Author contributions:** E.M. originated the concept for the study. A.S. and E.M. manufactured G-biointerfaces, performed experiments, analyzed the data, and wrote the manuscript. V.C. wrote automated image analysis software and analyzed the data. C.L. and A.K. performed experiments. G.B.B. produced rGO and manufactured G-biointerfaces. Y.I.M. participated in designing zebrafish experiments. All authors participated in manuscript revision. **Competing interests:** E.M. is an inventor on a pending patent application related to this work (PCT/US2015/035622, priority date: 17 June 2014). The authors declare that they have no other competing interests. **Data and materials availability:** All data needed to evaluate the conclusions in the paper are present in the paper and/or the Supplementary Materials. Additional data related to this paper may be requested from the authors.

Submitted 17 January 2018
Accepted 29 March 2018
Published 18 May 2018
10.1126/sciadv.aat0351

Citation: A. Savchenko, V. Cherkas, C. Liu, G. B. Braun, A. Kleschevnikov, Y. I. Miller, E. Molokanova, Graphene biointerfaces for optical stimulation of cells. *Sci. Adv.* **4**, eaat0351 (2018).